International Journal of Heat and Technology
Vol. 42, No. 2, April, 2024, pp. 593-602
Journal homepage: http://iieta.org/journals/ijht

Thermal Performance Analysis of Thermosyphon Solar Water Heating System Using Overlapped and Reverse Flow

Abdulaziz A. Moshab, Ra'ad K. Mohammed Aldulaimi*

Department of Mechanical Engineering, Al-Nahrain University, Baghdad 10072, Iraq

Corresponding Author Email: raad.K.mohammed@nahrainuniv.edu.iq

https://doi.org/10.18280/ijht.420226

Received: 8 November 2023
Revised: 14 March 2024
Accepted: 22 March 2024
Available online: 30 April 2024

Keywords:
flat plat collector, heat transfer enhancement, overlapping and reversed flow

ABSTRACT

A suggested absorption tube was designed for a thermosyphon solar water heating system (TSWHS) to enhanced the ability of the solar receiver to capture solar energy. The proposed design was based on overlapping and reversed flows, and its correctness was confirmed by conducting experimental simulations of the incident solar radiation and projecting heat flux on the proposed receiver tube models (Rt). Five receiver tube models were proposed as the standard, designed, and manufactured models which were tested under constant boundary conditions for all modeled flow rates (100, 150, 200, and 250 mL), flow directions (p_x and p_y), and constant heat flux. The most favorable thermal enhancement outcomes were achieved with the Rt_4 model that exhibited a thermal efficiency of 70.5%, featuring an inner tube diameter of 12 mm and outer tube diameter of 35 mm, incorporating a p_y flow path. The selected model (Rt_4) was employed, utilizing a p_y flow path for manufacturing the flat-plate collector (SRT_2). The model was then compared with a normal model (SRT_1) through Tests that were conducted for each model under similar weather conditions. The thermal gradient within the horizontal tank displayed an improvement by increasing 17% in heat transfer compared with the normal model.

1. INTRODUCTION

Solar energy is a highly efficient renewable energy source, with research supporting its various applications ranging from industrial water pumping to residential water heating, cooling, and cooking. Solar water heaters are gaining popularity globally owing to their reliability and affordability. Among the techniques employed, thermosiphon solar-powered water heaters are simple and cost-effective, promoting their widespread use in households and agriculture.

Over time, advances and experiments further enhanced the performance of thermosyphon water heaters. These systems offer numerous advantages over forced circulation alternatives, including independence from pumps and controllers, improved reliability, and extended lifespans. This underscores the practicality and suitability of their widespread adoption in diverse settings.

2. LITERATURE REVIEW

2.1 Improvement in the tube geometry

Aldulaimi [1] conducted an experiment to determine the values of Nu and EEC, as well as the temperature and pressure differentials in fluid flow. This study examined the production of reverse and overlapping flows in parabolic and trough collectors by inserting a twisted tube at the center of a circular tube in a variety of configurations. The novel design was validated using five receiver tube (Rt) models, each with two types of overlapping flows. The best model, which used a different mass flow rate, outperformed the regular model by 42.917%-38.528%.

Ayompe and Duffy [2] used information from a field examination that lasted for one year. The thermal efficiency of a solar water heating system with a heat-pipe evacuation tube collector was examined. An automated subsystem for managing hot water draw-offs and electric immersion heaters was designed and installed to mimic the functioning of residential solar water heating systems. The yearly average daily energy production was 20.4 MJd^{-1}, and the system efficiency was 52.0%.

Yang et al. [3] conducted a series of experiments to enhance the heat transfer performance of two types of molten salt receiver tubes, namely smooth and spiral tubes, under conditions of high temperatures and high heat flux. The experimental results indicated that the Nusselt numbers for the spiral tube with heat transfer improvement ranged from 400 to 1200. These findings suggest that using a spiral tube as part of the heat transfer system significantly improved the performance of the molten salt receiver and reduced radiation and conduction losses.

Rodríguez-Sánchez et al. [4] conducted a year-long field trial to investigate the thermal efficiency of a solar water heating system employing a heat pipe evacuation tube collector. To mimic the typical operation of household solar water-heating systems, an automated subsystem was devised and installed to manage hot water withdrawal and electric

immersion heaters. The system exhibited an efficiency of 52.0% and an average daily energy production of 20.4 MJ d-1 over a year.

Ananth and Jaisankar [5] used laminar flow conditions to examine the heat transfer and friction factor properties of solar water heaters fitted with twisted inserts comprising rods and spacers of various sizes. The findings showed that, while the collector performance indicator, the heat loss coefficient, increased, the heat removal factor decreased as the lengths of the rods and spacers increased. Moreover, twisted inserts with rods exhibited a more substantial improvement in heat transfer than those with spacers. Under the same operational conditions, the thermal efficiency of the best-performing model (a completely twisted tube) was 1.15 times higher than that of a standard flat-plate collector (FPC) with a plain tube.

Saravana et al. [6] analyzed the heat transfer and friction factor characteristics of V-trough solar water heaters (SWHs) fitted with helical twist tapes with different twist ratios (Y=3, 4, 5, and 6), including experimental research. The results showed that, in comparison with a flat-plate collector, the V-trough reflector increased the heat transfer efficiency by 13.64%. Moreover, the thermal efficiency of the V-trough collecting tube equipped with the twisted tape, which had a lower twist ratio of 3, was 5.41%, 9.91%, 14.77%, and 18.91%, respectively, greater than the thermal efficiency with twist ratios of 4, 5, 6, and without the twisted tape (PVT collector).

Jaisankar et al. [7] conducted an experimental examination of thermosiphon water heating systems (TSWHS) equipped with helical and left–right twisted inserts with a twist ratio of three. The left–right system provides a two-way swirling flow, which resulted in increased heat transmission and pressure loss compared with the helical system. The helically twisted insert created a one-way swirling flow along the riser tube. The left–right twisted insert collector exhibited a notable enhancement as compared with a simple tube collector; its heat transfer and friction factor were 3.75 times (375%) and 1.42 times (142%) greater, respectively.

Barbosa et al. [8] designed and tested two economical solar heating systems (ESHs) for thermal assessment. Their setups incorporated flat-panel solar collectors and heat storage components, which were constructed from PVC tubing, bottle caps, and durable packaging materials. Three temperature readings were recorded. When compared with the LCSHS, the LCSHP exhibited more outstanding performance. The highest temperatures and efficiency values for LCSHP were 49.7℃ and 40.9%, respectively, and those for LCSHS were 47.8 ℃ and 37.8%, respectively.

Wenceslas and Ghislain [9] utilized optimization findings to construct a flat-plate solar collector using locally accessible materials. A genetic algorithm was used to write the computer code, which assisted in obtaining the optimal combination of design parameters that optimized the exergy efficiency. The highest energy efficiencies obtained via the experiment and simulation were 68.71 and 66.01%, respectively, whereas the maximum energetic efficiencies were 20.34 and 18.65%, respectively.

Jawad et al. [10] used an experimental setup comprising a pair of copper tubes arranged in a dual-spiral configuration, with the inner surface of the solar collector coated in matte black paint containing a 5% blend of nanomaterials alongside a thermoplastic dye (TiN). The investigation reported a close correspondence between the theoretical predictions and analytical outcomes, indicating a strong agreement between the two sets of results.

Amraoui [11] compared two solar collector designs, with a focus on enhancing Ben Slama Romdhane's collector by introducing two additional airflow passages to boost the heat transfer. They conducted a 3D simulation of a flat air solar collector featuring transverse baffles to induce turbulence and augment the exchange surface area. The ANSYS computational code facilitated swift and cost-effective simulations, yielding prompt results.

2.2 Improved with coating

Sahu et al. [12] developed a novel and affordable combination of Fe and Mg. These coatings were specific to flat-plate absorbers of solar water-heating systems. Various analytical methods were used to characterize the composition of the coating mixtures. Two solar-collector prototypes were built. Fe-modified black paint had better excellent thermal absorption, with FPA2 having a 60% efficiency compared with FPA1's 48%.

Zelzouli et al. [13] found that a horizontally oriented storage unit with low wall conductivity could be merged with a flat-plate collector with a selective black-chrome-coated absorber. These findings indicate that polyurethane is a highly effective material for insulating thermal systems. A 2% enhancement in annual performance was achieved by reducing the collector's heat loss coefficient by 1 W/m² K.

2.3 Improvement in the geometry of solar panels

Lu et al. [14] created dynamic models to predict the thermal efficiency of a residential thermosyphon solar water heating system. A dedicated outdoor experimental setup was devised to confirm the accuracy of the model. The optimal airgap thickness for the thermosyphon solar water heating system was 25 mm, as this was the point at which heat loss through the glass cover plate stopped decreasing. Furthermore, both the energy loss and ultimate water temperature in the tank decreased as the water tank volume increased.

Khalifa et al. [15] developed a thermal storage solar collector composed of six 80-mm-diameter copper pipes linked in series. This collector was used in conjunction with a rear container that held paraffin wax, which served as a phase change material (PCM) to store heat. The ability of the system to heat water is verified through outdoor trials. The temperature of the plate increased at a distance of 2.5 m from the entrance site before stabilizing. The storage system's immediate efficiency varied between 45% and 54%.

2.4 Solar panel tank improvements

Zhang et al. [16] calculated the yearly performance of two-loop thermosyphon (LT) systems using the traditional SWH system investigated in this study. The supply duration, heat gain, and nocturnal heat loss were evaluated for two operational scenarios. They revealed that, based on calculations, the annual average heat loss ratio for the SWH system was 15.07%, whereas that for the LT-SWH system was 6.15%.

Naveen et al. [17] conducted a comprehensive stratified experimental investigation of heat energy-storage tanks in SWHs. Their study encompassed tanks with various configurations, including those without a PCM, those with a PCM but lacking fins, those with a PCM featuring ring-type fins, and those equipped with spiral fins. In each scenario, the

efficiencies of hourly charging and discharging were assessed and juxtaposed. The highest charging efficiencies observed in the PCM were 71% for the spiral module, 66% for the cylindrical PCM module without fins, and 58% for the cylindrical PCM module with fins.

3. METHODOLOGY

To accelerate the rate at which heat is transferred from solar radiation to the heat-transfer fluid (HTF), a new SWHS model based on overlapping and reversed tubes was proposed to increase the fluid path inside the tube, which led to increased absorption of solar energy falling on the solar collector. This led to an increase in the absorption of thermal energy. This model was applied with different internal tube diameters by simulating the process of incident solar energy. After selecting the optimal model in terms of thermal optimization, the solar heater was manufactured and the thermal performance was studied.

The solar energy simulation was performed using a flat heater (120×1000 mm) based on a parabola-shaped reflector. This reflector reversed the heat flux and prevented dispersion. The tube models were exposed to a heat flux. Four overlapping and reversed tube models (Rt2, Rt3, and Rt4) were used. After optimizing the model from the simulation (Rt4), fins were added to the outer surface of the inner tube to increase heat transfer, resulting in the creation of a fifth model (Rt5). The revised design maintained a constant outer tube diameter (Tu1). However, the inner tubes' diameters (Tu2, Tu3, and Tu4) were altered, allowing for comparisons between them and against the standard model (Rt1) while maintaining the exact measurement of the outer diameter in the proposed designs.

After determining the model that provided the best thermal improvement, a solar collector model was designed and manufactured for overlapping and reversed tubes with the same diameter as the model that provided the best efficiency. The proposed model consisted of ten pipes compared with the normal model to be presented with solar radiation to verify the proposed and manufactured thermal efficiency.

4. EXPERIMENTAL SYSTEM DESCRIPTION

4.1 Experimental simulation system

Figures 1 and 2 show a visual illustration of the model and a schematic of the device, respectively. Solar energy simulation relies on simulating the transfer of solar energy to a solar receiver through radiation, which is simulated in a laboratory [3]. The simulated model included a thermal heating element that was used to simulate solar energy to stabilize the thermal energy and change the mass flow rate. It was installed on a structure composed of parabolic steel to reverse the heat flow toward the pipe and prevent significant heat losses. The thickness of the steel sheet was 1 mm and the width was 300 mm with the extension of the device (Table 1). The heater was connected to a variable-voltage device (TDGC-series Contact Voltage Regulator). The tube model was fixed 20 mm from the surface of the heater using the second steel ring connected to the structure of the external device. The four models and normal model were applied to the heat flux. The flow in progress was measured once for the px flow and again for the py flow. A flowmeter was used at the exit point to control the fluid flow velocity. Four different fluid flow rates were recorded for each model. K-type sensors were positioned at the entry, exit, and reflection points along the direction of the HTF, and one sensor was installed on the outer surface of the outer tube to measure the surface temperature. The heat data collected were recorded using twelve-channel, TM 500-model thermal data recorder. The readings recorded by the data logger were stored on an SD card placed inside the recorder and extracted using a computer. Readings were taken after reaching stability at five-minute intervals, and the device was calibrated with another approved meter before use. A differential pressure manometer with 1-mbar precision was used to detect the pressure differential within the Rt.

Figure 1. Simulated solar collector

Table 1. The characteristics of the simulation system

Feature	Value	Feature	Value
Aperture area, A_a	0.12 m^2	Length, l	1 m
Receiver area, A_r	0.11m^2	Aperture width, W_a	0.035m
Material of the tubes	copper	Working fluid	Water
Direct heat flux, I_{dth}	1000 W		

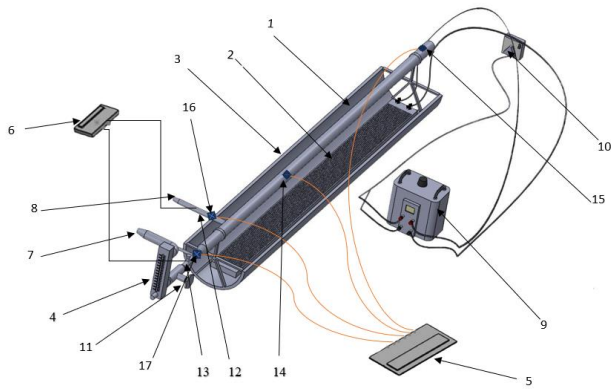

1. receiver tube (Rt), 2. electrical flat heater, 3. steel reflector, 4. micro-flowmeter, 5. data logger, 6. differential pressure manometer, 7. p_x flow, 8. p_y flow, 9. contact voltage regulator (TDGC series), 10. electrical source, 11. valve, 12. inlet fluid pressure measurement point, 13. outlet fluid pressure measurement point, 14. thermocouple sensors for surface temperature, 15. temperature of the reverse fluid flow measurement point, 16. inlet fluid temperature measurement point, and 17. outlet fluid temperature measurement point.
Note: The schematic represents the third model (Rt_4) and p_y flow

Figure 2. Schematic of the experimental simulation system

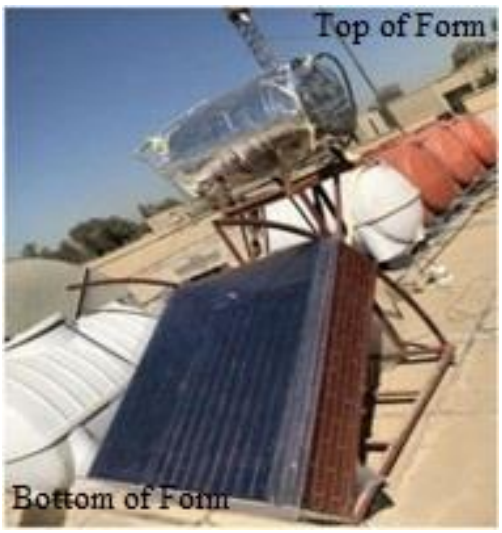

Figure 3. Photograph of (TSWHS)

4.2 Description of the TSWHS

The system is depicted in Figure 3 and an explanatory diagram is presented in Figure 4. Once the experimental verification was completed and the model that exhibited the best thermal performance was identified, an experimental investigation was initiated for the flat-plate collector system (FPCS). This system was constructed using interconnecting and reverse-oriented tubes along with a standard model for comparative purposes. Copper was chosen as the material for the tubes due to its high thermal conductivity (386 W/m^{2}K) and significant melting point of 1000 °C. Water was used as the operating fluid. The experimental model comprised a frame supporting the SWH models and a storage tank with a capacity of 196 L. The frame was constructed from iron and insulated with two layers of wood and glass fibers to encompass the solar receiver, thereby reducing heat loss. The dimensions of the frame were 1020×1190 mm with a height of 25.5 cm and an insulator width of 5 cm. The tank was installed at the top of the frame and was completely insulated using fiberglass. The external surfaces of the solar collectors were coated with charcoal-black paint to enhance their absorption properties. The K-type thermocouples were attached to the inlet and outlet of the HTF, and six additional K-type thermocouples were positioned on the outer surfaces of the SRT models. Two sensors were inserted in the storage tank to measure the thermal gradient within the tube. Additional details are provided in Table 2.

Table 2. Physical specifications of the solar water heating system

Feature	Value	Feature	Value
Title angle	33º	Aperture area, Ac	0.8 m^2
Collector glazing	Single transparent glass of 4 mm	Transmittance of glazing	0.91
The upper header for the SRT1 collector	35 mm	The lower header for SRT1	35 mm
The inlet header for SRT2	16 mm	The outlet header for SRT2	16 mm
Number of riser tubes for SRT1, SRT2	10	Absorber plate	Width 122 mm, length 1000 mm
The maximum I_d	803 W/ m^2	Side and bottom insulation	60 mm glass wool
Tank type	Horizontal tank	Tank volume	196 L
Tank insulation thickness	60 mm of glass wool	Pipe insulation thickness	20 mm

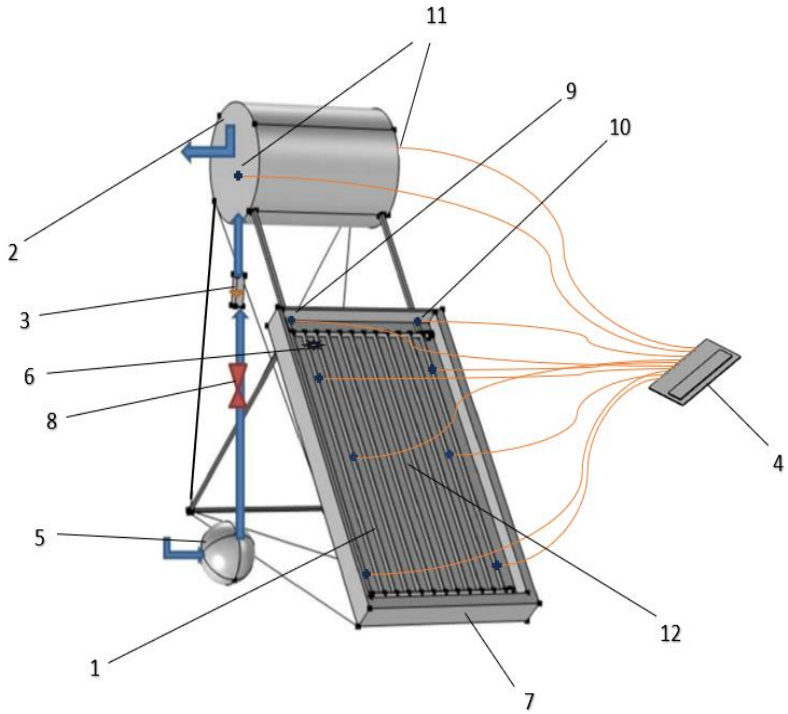

1. Solar collector, 2. horizontal tank, 3. flow meter, 4. data logger, 5. pump, 6. solar intensity sensor, 7. insulation supported by wooden frame, 8. valve, 9. inlet fluid temperature measurement point, 10. outlet fluid temperature measurement point, 11. two thermocouple sensors for tank temperature, 12. one of the six thermocouple sensors for the surface temperature. Note: Schematic represents the normal model (SRT_1).

Figure 4. Schematic of the experimental system

5. TECHNICAL DETAILS OF THE MODELS

5.1 Technical details for simulation system (Rt models)

Five Rt models were used in this experimental simulation, depending on the inflow from the central or peripheral pipes, to determine the most improved heat transfer. They had various arrangements based on overlapping and reversible flows. Each proposed Rt was built using a three-tube model with varying hydraulic diameters Hd, in addition to the normal model with the normal-shaped tubes. A constant outer tube diameter was used in all models, as shown in Figure 5(a). Tubes (Rt2, Rt3, and Rt4) with inner tubes of different diameters (Tu1, Tu2, and Tu3) are shown in Figure 6.

Model Rt4 was the most efficient, with the highest thermal enhancement. To improve the heat transfer, fins were added to the outer surface of the inner tube, resulting in the development of the fifth model, Rt5, as shown in Figure 5(b). Measurements were taken for various parameters, including temperature difference (ΔT), temperature at the reflection point in the flow direction, average surface temperature for each Rt model, and flow rate. Additionally, the pressure drop was calculated.

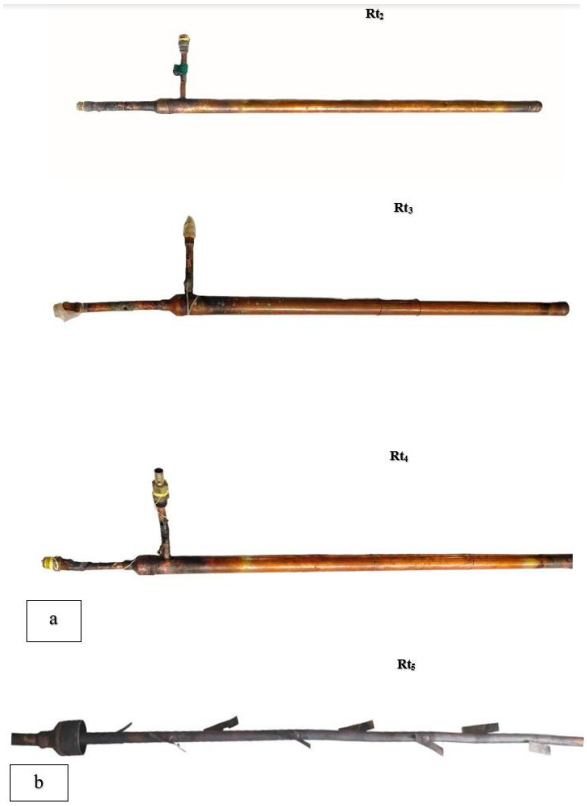

Figure 5. (a) Photographs of models Rt_2, Rt_3, and Rt_4; (b) Photograph of the inner tube (Tu4) after adding fins to the outer surface

5.2 Technical details for SRT models

In this experimental study, two models are designed and manufactured (SRT), and the area of the solar collector is (0.957) m^2. The front is insulated using transparent glass to prevent heat losses, while the other sides are insulated using wood and glass. The solar collector is linked to a 196-liter tank horizontally installed. Both are effectively insulated using glass wool. The system is installed firmly to an iron frame. The models have been painted charcoal-black to improve the absorption of solar energy. The normal model (SRT_1) consists of ten tubes. The tube model is Rt1, as shown in the Figure 7.

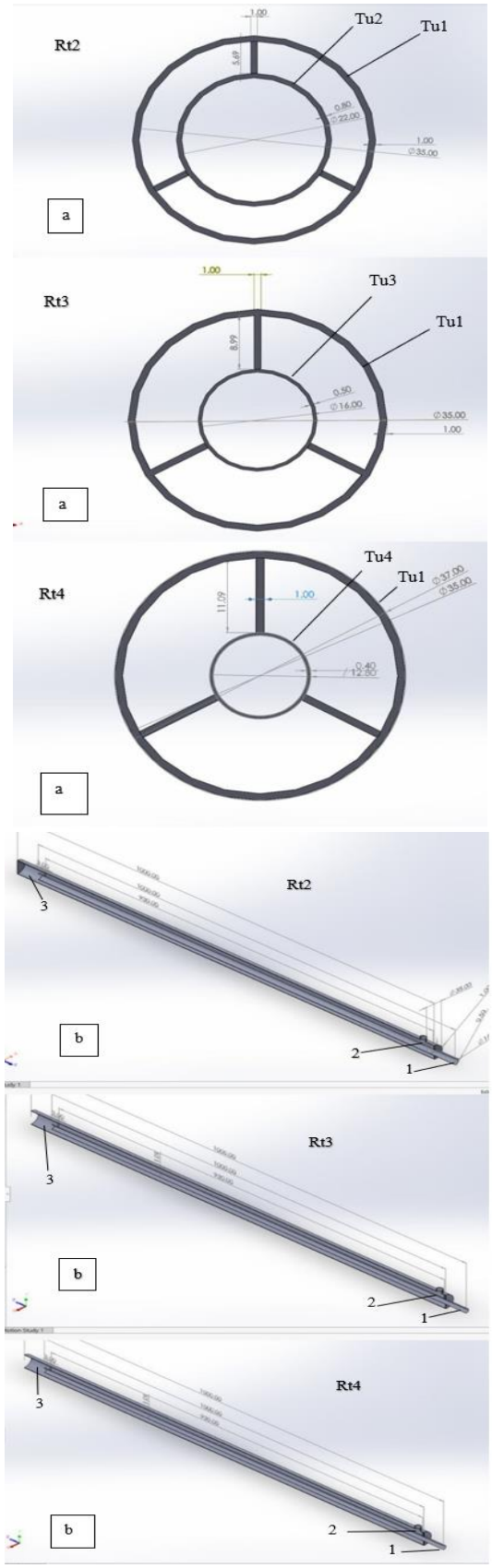

Figure 6. (a) Detailed cross-section of the received tube model Rt; (b) scheme of the Rt2, Rt3, and Rt4 models. 1. P_x flow path, 2. P_y flow path, 3. The point of reflection of the fluid flow

Figure 7. Phytophagic of solar collector models (FPC): (a) SRT_1. 1 and 2, Inlet or outlet fluid; (b) SRT_2. 1 and 2, Inlet or outlet fluid

The second model is the proposed (SRT_2) model. The tube model is Rt4, and the flow path is pry, which gives the best thermal performance. It also consists of ten tubes, as shown in the Figure 7.

6. EXPERIMENTAL SETUP AND TEST PROCEDURE

6.1 Simulation system experimental setup and test procedure

A practical simulation was performed in the laboratories of the Al-Nahrain University College of Engineering. The test was conducted from March 3-15, 2023, with an average maximum atmospheric temperature of 21°C. Readings were taken at 5-min intervals after reaching stability, typically approximately half an hour after activating the heater and systematically logged using a data logger. A minimum of four temperature readings were collected for each flow rate, including measurements of the entry-point temperature, point of reflection of the fluid flow, exit-point temperature, surface temperature of the pipe, and ambient temperature. The experimental simulation started with one flow path (p_x) and then switched to another (p_y) with four mass flow rates (100, 150, 200, and 250 mL/min) for each flow path. Measurement points were placed at the entrance and exit to continuously measure the differential pressure, which changed with the change in flow rate.

6.2 Experimental setup and test procedure for the experimental system (TSWHS)

Practical experiments were conducted at Baghdad's Al-Nahrain University within the College of Engineering (located at a latitude of 33.27°N and longitude of 44.38°E in Al-Jadira, Baghdad). These experiments were conducted from May 18-22, 2023, under clear weather conditions. During the measurements, the maximum temperature reached 41°C, with a relative humidity of 22.6% and average wind speed of 2.1 m/s.

Several measurements were conducted, including the inlet and outlet temperatures, as well as the temperatures at six specific points on the external surface of the Rt models. Furthermore, the temperature gradient within the tank was determined using two embedded thermocouples, and the average surface temperature for each Rt model and flow rate were computed. Temperature data from all the thermocouples were recorded every 60 s using data loggers over a 24-h period. The solar radiation intensity was also monitored with data loggers every 30 s, capturing the radiation levels per second over the course of 24 h. The choice of the flow path (py) was determined based on the proposed model because it exhibited the highest thermal efficiency.

7. DATA PROCESSING

7.1 Collector efficiency

The heat transfer rate (Q_u) within Rt was based on the HTF and can be expressed as follows [10]:

$$Q_u = \dot{m}_{HTF}\, c_p\, (T_{out} - T_{in}) \quad (1)$$

where, the specific heat capacity (c_p) is calculated as a function dependent on the average temperature of the Rt.

The η was defined as:

$$\eta = Q_u / (I_d\, A_a) \times 100\% \quad (2)$$

where, I_{dth} is the direct heat flux of the thermal heater.

7.2 Heat transfer

According to Ananth and Jaisankar [4], (Q) can also be estimated by:

$$Q = U_{wo}\, A_{wo}\, (T_{wo} - T_m) \quad (3)$$

where, T_m is the Temperature of the reverse fluid flow.

Also [5]:

$$\frac{1}{(U_{wo}A_{wo})} = \frac{1}{h_{wi}\, A_{wi}} + \frac{\ln(D_o/D_i)}{(2\pi k_w l)} \quad (4)$$

Eq. (4) has the following form:

$$h_{wi} = \left[\left(\frac{1}{(U_{WO}A_{wo})} - \frac{\ln(D_o/D_i)}{(2\pi k_w l)}\right) \times A_{wi}\right]^{-1}$$

Eqs. (1), (3), and (4) are used to yield the experimental Nu as:

$$\mathrm{Nu} = \frac{h_{wi}D_i}{K_{HTF}} \quad (5)$$

At the temperature of reflection fluid Tm, the fluid's thermophysical characteristics are established.

7.3 Efficiency evaluation criterion (EEC)

The effective efficiency coefficient (EEC) was calculated and defined as per [1] to conduct a comprehensive assessment of the heat transfer improvement. This calculation involved comparing the new Rt models with the standard Rt, while considering identical pumping power consumption and operational parameters. This is a widely used criterion for evaluating different types of heat exchangers, with higher thermal enhancement index (EEC) values indicating superior thermal performance considering pumping power consumption.

$$EES = \frac{Q/Q_o}{\Delta p/\Delta p_o} \quad (6)$$

where, ($Q_o, \Delta p_o$) represents the (Q) and (Δp) in the Rt_1 model.

8. RESULTS AND DISCUSSION

The results of the experimental investigation indicated that, in comparison with conventional Rt models, there were enhancements in temperature difference (ΔT), Nusselt number (Nu), efficiency (η), and EEC when the mass flow rate (ṁHTF) was in the range of 0.00167–0.00416 kg/s. When expressed as a percentage, these improvements clearly highlighted the differences between the average Rt and the improved models. The practical results showed that, when we compared the improved TSWHS model with the normal one, there was a difference in the thermal gradient inside the tank, which improved the thermal performance of the system. The maximum uncertainties for the five parameters referred to above were approximately ±0.81°C, ±2.23 mbar, ±2.5%, ±2.87%, and ±2.125%, respectively, after calibration of the devices used for measurement.

8.1 Experimental simulation results

8.1.1 Temperature difference

In all the simulated models, the temperature difference and pressure decreased as the mass flow rate increased, as depicted in Figure 8. All the greatest differences in temperature were obtained (15.6-11.8°C) in model Rt_4 compared with the ordinary model Rt_1 (10.1-4.2), with flow path p_y and hydraulic diameter H_d of 1.27, which increased by 54.4-180.8%. To alter the fluid motion and swirl movement of model Rt_4, fins were added to the outside surface of the inner tube (model Rt_5), but the temperature difference increased (13.6-10.7°C) with flow path p_y, which was less than that of model Rt_4, with an increase of 34.6-154%. These results were all obtained for the same range of $\dot{m}_{HTF}$ (0.001667-0.004167 kg/s) and indicate an increase in energy absorption in the selected models.

8.1.2 Pressure difference

Figure 9 indicates a rise in the pressure variation (19-6 mbar) for model Rt_4 at flow path p_x, representing a power difference (137-100%) for the range $\dot{m}_{HTF} = 0.001667 - 0.004167\ kg/s$, when compared with model Rt_1, which indicated a pressure difference (8-3 mbar) for the same $\dot{m}_{HTF}$ range; the largest pressure difference (22-12 mbar) occurred for model Rt_5 with a flow path p_x, which increased by 175-300%. This increase occurred because of the increased friction and subsequent elevated pressure losses in the system. Increasing the pressure difference loss led to an increase in the energy expended during the movement of the fluid.

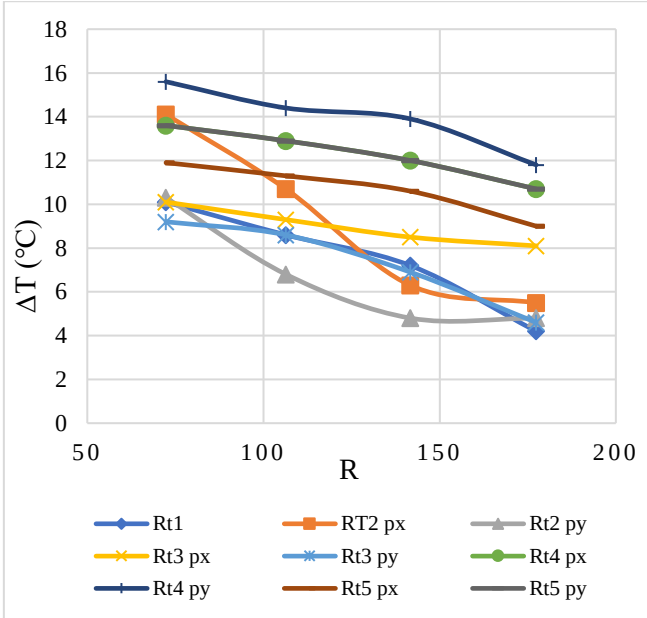

Figure 8. The relationship between reynolds number and the temperature difference ΔT (°C) for all Rt models

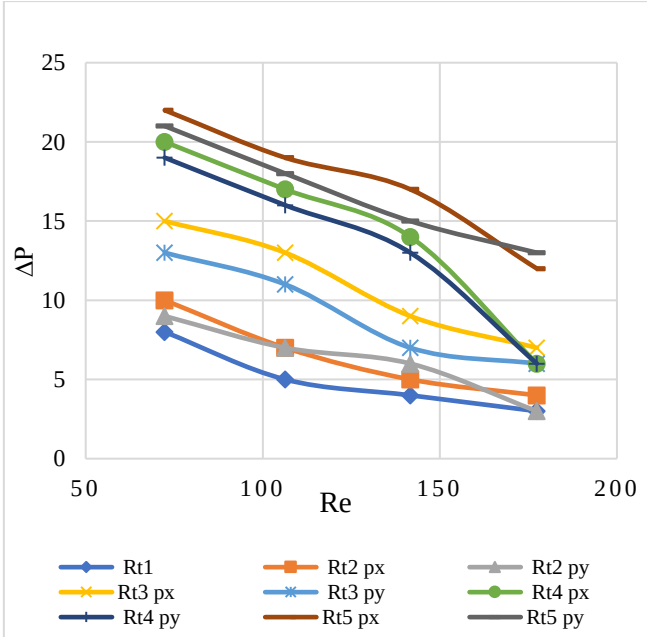

Figure 9. The relationship between the Reynolds number and the pressure difference (ΔP m bar) for all Rt models

8.1.3 Collector efficiency η

For each R_t model and flow rate, calculations were performed using Eq. (2), as shown in Figure 10. There was an increase in efficiency with a decrease in mass flow rate ($\dot{m}_{HTF}$). The maximum η value occurred for model Rt_4 (37.3-70.5%) for a flow path p_y, which increased by 14.7-67.8% compared with the normal model Rt_1, which had an efficiency of 24-42.8%. This amounted to a 42.917-38.528% increase. All of

these values were for the same range ($\dot{m}_{HTF} = 0.00167 - 0.00167\ kg/s$).

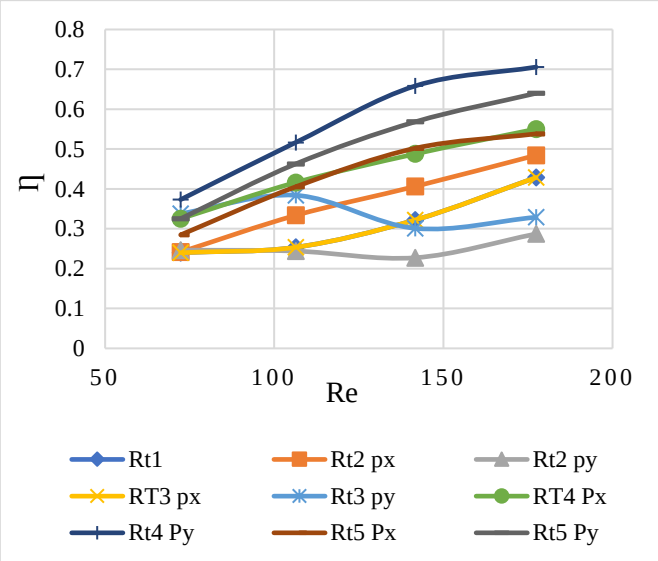

Figure 10. The mean collector efficiency (η) values for all models of (Rt)

8.1.4 Nusselt number *Nu*

Figure 11 shows that the Nusselt number (Nu) gradually decreased with an increase in the mass flow rate. This trend can be attributed to a reduction in the heat transfer rate and the relative stability of the surface temperature beyond a certain rate. Nu was estimated for each R_t model. The highest Nu value was obtained for model Rt_4 (17.02-13.7) with the flow path of p_y compared with the normal form Rt_1 (9-7), where an increase of (89–95%) represents the highest increase obtained.

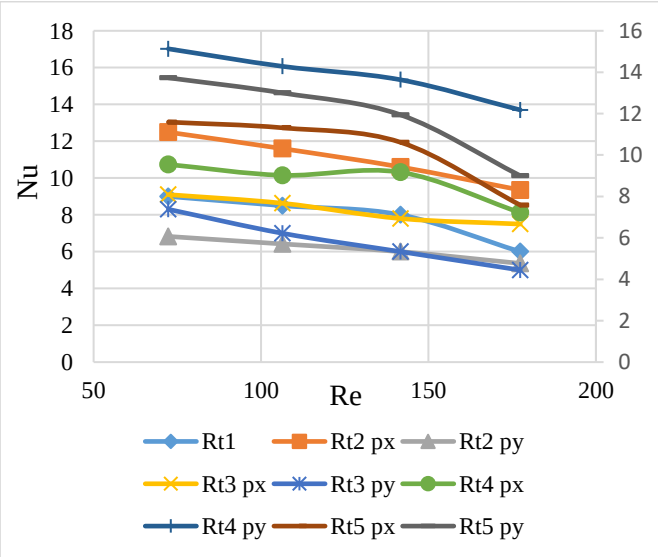

Figure 11. The relationship between mass flow rate and Nusselt number (Nu) for all Rt models

8.1.5 Efficiency evaluation criterion EEC

The EEC was computed using Eq. (6) to gauge the overall performance of the heat transfer unit, as explained in [1]. The results are presented in Figure 12. The findings indicated that the EEC increased notably as the flow rate increased, primarily because of the decrease in pressure loss at higher flow rates. Model Rt4 with the flow path py achieved the highest EEC value (ranging from 0.53 to 1.4), while model Rt5 with the flow path px recorded the lowest EEC value (ranging from 0.43 to 0.53). This considerable increase in pressure loss had a pronounced impact on the final EEC value.

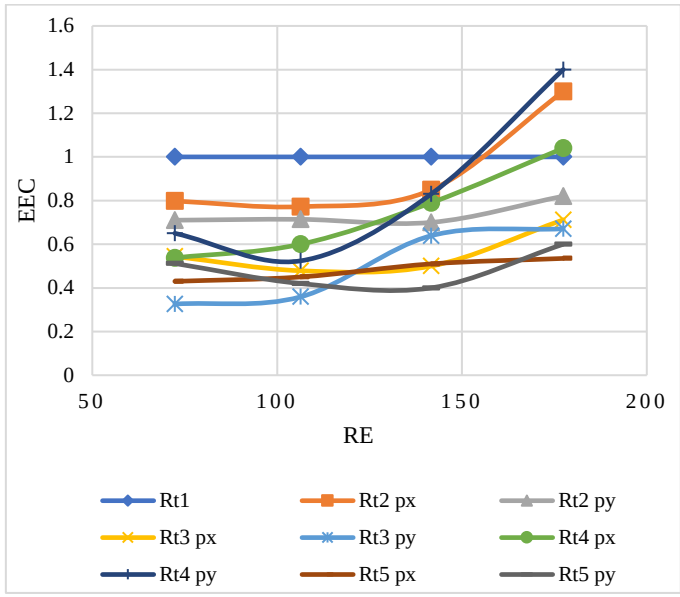

Figure 12. The relationship between mass flow rate and efficiency evaluation criterion (EEC) for all models of (Rt)

8.2 Experimental results

8.2.1 Temperature gradient

The experimental findings showed an enhancement in the heat transfer rate within the solar receivers. The normal model (SRT_1) and improved model (SRT_2) were compared, as shown in Figure 13. The thermal gradient inside the horizontal tank was calculated, and the results were recorded for an entire day under similar weather conditions. The highest thermal gradient value (58.4℃) was obtained for the normal model (SRT_1) at (12:16 PM), while the greatest thermal gradient (68.8℃) was recorded in the improved model (SRT_2) at (12:16 PM). A thermal improvement of 17.8% was achieved ($\frac{\overline{T}_{Tank\ SRT2} - \overline{T}_{Tank\ SRT1}}{\overline{T}_{Tank\ SRT1}} \times 100\%$). This outcome is primarily contingent on the intensity of incident solar radiation on the TSWHs.

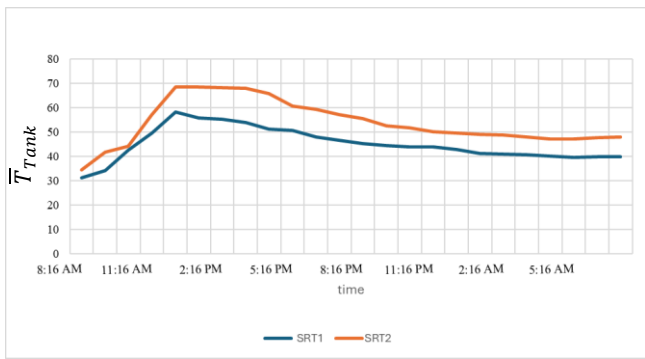

Figure 13. The relationship between the time of the whole day and the temperature inside the tank

8.2.2 Direct solar radiation

The solar radiation intensity incident on the solar collector was monitored continuously for an entire day, spanning 24 h, and the data logger was used to measure the values and record the data. Values were recorded every 30 s starting at 8:16 AM and ending at 7:16 AM. The highest solar radiation intensity (803 W/m^2) was recorded at 12:16 PM, as shown in Figure 14. This value was obtained because of solar orthogonality, the highest value of which occurred at this time.

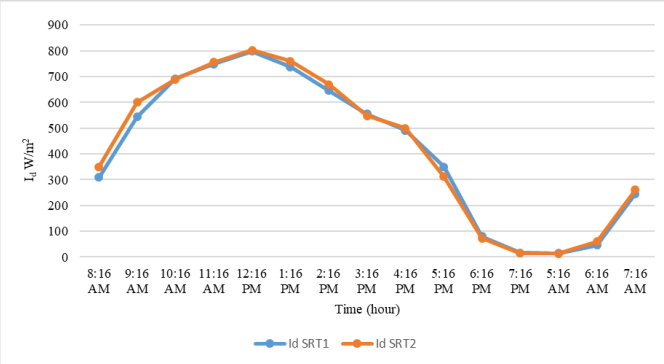

Figure 14. The relation between the time of the day and the intensity of the solar radiation

9. CONCLUSION

A new technique was applied to a TSWHS, and experimental verification was performed in two parts. The first experimental verification involved determining the temperature and pressure difference of the fluid flow, η, Nu, and EEC by performing an experimental simulation of the solar radiation incident on the solar collector. A set of proposed tube models was used and exposed to heat flux, overlapping, and reverse flows. It was constructed using a normal round-tube model in another round tube with different hydraulic diameters (Hd) for the proposed models. Three internal tube diameters were used (22, 16, and 12 mm) and the tubes were selected according to market availability for the geographical area where the test was conducted; two types of path flow were used, the first from the inner tube to the outer tube (p_x), and the other from the outer tube to the inner tube (p_y). The best thermal improvement occurred in model Rt4 with flow path py. The reason for the effect of changing the flow rate on ΔT, i.e., the slower the mass flow rate, provides sufficient time for the fluid molecules to gain energy, leading to an increase in the temperature difference by decreasing the flow rate. Fins on the outer surface of the inner tube were added to model Rt4 to form model Rt_5 in order to increase the adhesion area between the fluid particles and metal to increase heat transfer and create a swirl inside the outer path of the model. This model increased the pressure difference, which led to a decrease in the EEC, but did not provide an additional improvement over model Rt4. Table 3 shows the enhanced heat transfer in the models.

In the second phase, an experimental analysis of a TSWHS was performed. The most effective model in terms of thermal performance (Rt_4) and the use of a p_y flow configuration were selected. This model was used as the basis for the development of a new solar collector model (SRT_2). Subsequently, the performance of SRT2 was assessed against that of a standard model (SRT1) under similar environmental conditions. The test was conducted over an entire day, during which the temperature gradient within the tank was measured. The findings revealed a 17% enhancement in heat transfer compared with the standard model. The novel design employing overlapping and reverse flow tubes demonstrated superior efficiency compared with the conventional model. Moreover, its operation without the need for external pumping power rendered it economical and highly efficient.

One avenue for future research could be to focus on enhancing the design of tubes to improve the heat transfer efficiency. This may involve exploring alternative materials with superior thermal conductivity, optimizing the geometry of the tubes, and investigating the impact of different fluid properties and operating conditions on the thermal performance of the system.

Table 3. The enhancement of (ΔT, ΔP, η and Nu) variables related to R_t models

	ΔT °C	ΔP mbar	η	Nu
Rt_1	Base model			
Rt_2 p_x	39.6-30.9%	25-33%	1-13%	38.77-55.9%
Rt_2 p_y	2-14.2%	12.5-0%	3-0%	0%
Rt_3 p_x	0-92.8%	87.5-133%	0-1%	1.11-25%
Rt_3 p_y	0-10%	62.5-100%	40.8-0%	0%
Rt_4 p_x	34.6-154.7%	150-100%	36-28.39%	19.31-35%
Rt_4 p_y	54.5-180.9%	137-101%	55.5-64.44%	89.11-128%
Rt_5 p_x	18-114.2%	175-300%	18.6-25.57%	44.87-42.1%
Rt_5 p_y	29-152%	162.5-333%	35.4-49.3%	52.55-50%

REFERENCES

[1] Aldulaimi, R.A.K.M. (2019). An innovative receiver design for a parabolic trough solar collector using overlapped and reverse flow: An experimental study. Arabian Journal for Science and Engineering, 44(9): 7529-7539. https://doi.org/10.1007/s13369-019-03832-8

[2] Ayompe, L.M., Duffy, A. (2013). Thermal performance analysis of a solar water heating system with heat pipe evacuated tube collector using data from a field trial. Solar Energy, 90: 17-28. https://doi.org/10.1016/j.solener.2013.01.001

[3] Yang, M., Yang, X., Yang, X., Ding, J. (2010). Heat transfer enhancement and performance of the molten salt receiver of a solar power tower. Applied Energy, 87(9): 2808-2811. https://doi.org/10.1016/j.apenergy.2009.04.042

[4] Rodríguez-Sánchez, M.R., Sánchez-González, A., Marugán-Cruz, C., Santana, D. (2014). New designs of molten-salt tubular-receiver for solar power tower. Energy Procedia, 49: 504-513. https://doi.org/10.1016/j.egypro.2014.03.054

[5] Ananth, J., Jaisankar, S. (2013). Experimental studies on heat transfer and friction factor characteristics of thermosyphon solar water heating system fitted with regularly spaced twisted tape with rod and spacer. Energy Conversion and Management, 73: 207-213. http://doi.org/10.1016/j.enconman.2013.04.022

[6] Saravanan, A., Senthilkumaar, J.S., Jaisankar, S. (2016). Experimental studies on heat transfer and friction factor characteristics of twist inserted V-trough thermosyphon solar water heating system. Energy, 112: 642-654. http://doi.org/10.1016/j.energy.2016.06.103

[7] Jaisankar, S., Radhakrishnan, T.K., Sheeba, K.N. (2011).

Experimental studies on heat transfer and thermal performance characteristics of thermosyphon solar water heating system with helical and left–right twisted tapes. Energy Conversion and Management, 52(5): 2048-2055. http://doi.org/10.1016/j.enconman.2010.11.024

[8] Barbosa, E.G., de Araujo, M.E.V., de Moraes, M.J., Martins, M.A., Alves, B.G.X., Barbosa, E.G. (2019). Influence of the absorber tubes configuration on the performance of low cost solar water heating systems. Journal of Cleaner Production, 222: 22-28. https://doi.org/10.1016/j.jclepro.2019.03.020

[9] Wenceslas, K.Y., Ghislain, T. (2019). Experimental validation of exergy optimization of a flat-plate solar collector in a thermosyphon solar water heater. Arabian Journal for Science and Engineering, 44(3): 2535-2549. https://doi.org/10.1007/s13369-018-3227-x

[10] Jawad, S.A., Rashid, F.L., Ridha, Z.A.A. (2022). Thermal performance of spiral flat plate solar water collector. International Journal of Heat and Technology, 40(1): 183-192. https://doi.org/10.18280/ijht.400122

[11] Amraoui, M.A. (2021). Three-dimensional numerical simulation of a flat plate solar collector with double paths. International Journal of Heat & Technology, 39(4): 1087-1096. https://doi.org/10.18280/ijht.390406

[12] Sahu, A.K., Brahma, G.S., Aravind, R., Swain, T. (2021). Thermal application of composites of iron and magnesium in thermosyphon solar water heating system. Heat Transfer, 50(8): 8617-8639. https://doi.org/10.1002/htj.22293

[13] Zelzouli, K., Guizani, A., Kerkeni, C. (2014). Numerical and experimental investigation of thermosyphon solar water heater. Energy conversion and management, 78: 913-922. https://doi.org/10.1016/j.enconman.2013.08.064

[14] Lu, L., Wang, X., Wang, S., Liu, X. (2017). Optimal structure design of a thermosyphon solar water heating system with thermal and dynamic models. Heat Transfer Engineering, 39(16): 1470-1481. https://doi.org/10.1080/01457632.2017.1379347

[15] Khalifa, A.J.N., Suffer, K.H., Mahmoud, M.S. (2013). A storage domestic solar hot water system with a back layer of phase change material. Experimental Thermal and Fluid Science, 44: 174-181. http://doi.org/10.1016/j.expthermflusci.2012.05.017

[16] Zhang, T., Yan, Z.W., Wang, L.Y., Zheng, W.J., Su, Y.H. (2020). Comparative study on the annual performance between loop thermosyphon solar water heating system and conventional solar water heating system. Solar Energy, 197: 433-442. https://doi.org/10.1016/j.solener.2020.01.019

[17] Naveen, T.K., Jagadesh, T. (2019). Experimental investigations into performance evaluation of thermosyphon solar heating system using modified PCM modules. In Advances in Fluid and Thermal Engineering: Select Proceedings of FLAME 2018, pp. 211-221. https://doi.org/10.1007/978-981-13-6416-7_20

NOMENCLATURE

A_a	Aperture Area (m^2)
A_{re}	Area of Receiver (m^2)
A_{wo}	Outer surface area of the receiver's outer tube (m^2)
A_{wi}	Inner surface area of the receiver's outer tube (m^2)
h_{wi}	Average convective heat transfer coefficient (W/m^2 °C)
D_i	Inner diameter of the outer tube of the receiver is typically measured in meters (m).
D_o	Outer diameter of the outer tube of the receiver is typically measured in meters (m).
D_{hi}	Inner hydraulic diameter of the inner tube of the receiver (m)
Qu	Rate of heat transfer (Q) within the receiver tube (Rt), which absorbs energy from the Heat Transfer Fluid (HTF), measured in kilowatts (kW).
$\dot{m}_{HTF}$	Mass flow rate of the water (kg/s)
T_{out}	Temperature at the outlet of the receiver tube (°C)
T_{in}	Temperature at the inlet of the receiver tube (°C)
T_m	The temperature of the point of reflection in the direction
T_{wo}	Average wall surface temperatures outside of the outer tube of the receiver (°C)
U_{wo}	Overall outside heat transfer coefficient for the outer tube of the receiver (W/m^2 K)
W_a	Aperture width (m)
Δp	Pressure drops (mbar)
I_d	Direct solar radiation (W/m^2)
I_{dth}	Direct heat flux (W/m^2)
k_w	Thermal conductivity of the outer tube of the receiver (W/m°C)
l	Length (m)
p_x	The path through which the flow moves from the inner tube to the outer tube.
p_y	Flow Path from the outer tube to the inner tube

Greek letters

θ	Title angle (º)

Abbreviations

FPCS	Flat plate collector system
TSWHS	Thermosyphon solar water heating system
HTF	Heat transfer fluid
Rt	The receiver tube of the simulation solar water heating system
Tu	The main tube holding the receiver tubes
SRT	Solar receiver of the flat plate solar collector
LCSHP	Low-cost solar heater in parallel
LCSHS	Low-cost solar heater in series
PVC	Polyvinyl chloride
PCM	Phase change materials